Liver X receptors in the central nervous system: From lipid homeostasis to neuronal degeneration

Ling Wang[‡], Gertrud U. Schuster[§], Kjell Hultenby[¶], Qinghong Zhang[‡], Sandra Andersson[‡], and Jan-Åke Gustafsson[‡§‖]

Departments of [‡]Medical Nutrition and [§]Biosciences, NOVUM, and [¶]Department of Clinical Research Center, Karolinska Institute, Huddinge University Hospital, S-141 86 Huddinge, Sweden

Contributed by Jan-Åke Gustafsson, August 23, 2002

Liver X receptors (LXRα and -β) are nuclear receptors abundant in the liver where they are regulators of lipid homeostasis. Both LXRs are also expressed in the brain, but their roles in this tissue remain to be clarified. We examined the brains of mice in which the genes of both LXRα and -β have been disrupted and found several severe abnormalities. One of the most striking features is that the lateral ventricles are closed and lined with lipid-laden cells. In addition, there are enlarged brain blood vessels, especially in the pars reticularis of the substantia nigra and in the globus pallidus. Other features of the brains are excessive lipid deposits, proliferation of astrocytes, loss of neurons, and disorganized myelin sheaths. Electron micrographs revealed that, as mice aged, lipid vacuoles accumulated in astrocytes surrounding blood vessels. Comparison of mRNA profiles in LXR knockout mice and wild-type littermates showed that expression of several LXR target genes involved in cholesterol efflux from astrocytes was reduced. These findings show that LXRs have an important function in lipid homeostasis in the brain, and that loss of these receptors results in neurodegenerative diseases. Further characterization of the role of LXRs in the brain could lead to new insights into the etiology and treatment of some neurodegenerative disorders.

The liver X receptors (LXRs) constitute a subfamily within the nuclear receptor superfamily of transcription factors. Two members of the LXR subfamily have been identified, LXRα and -β, and comparison of their sequences shows that human LXRα and -β share 77% amino acid identity in both their DNA- and ligand-binding domains. There is also a high degree of conservation of the LXRs between rodents and human (1). The major function of the LXRs in the liver is in regulation of lipid and lipoprotein metabolism. These receptors are activated by naturally occurring oxysterols, the best-studied and most potent of which include 24(S)-hydroxycholesterol, 22(R)-hydroxycholesterol, 24(S), 25-epoxycholesterol, and 27-hydroxycholesterol (2–4).

Cholesterol is a major lipid component of mammalian cell membranes (5) and is an obligate precursor of steroid hormones and bile acids. Several genes involved in cholesterol (6) and fatty acid metabolism (7, 8) have been found to be regulated by LXR. Some of these genes are: cytochorome P450 7A1, the rate-limiting enzyme in bile acid biosynthesis in the liver; the sterol regulatory element-binding protein-1 (SREBP-1); acetyl CoA decarboxylase; fatty acid synthase; and several ATP-binding cassette transporter proteins (ABCs) (9–15). LXRs also promote the transcription of the cholesterol ester transfer protein, lipoprotein lipase, and apolipoprotein (Apo)E (10). The human LXRα gene is itself a target of the LXR signaling pathway (16). Thus, the LXRs act as cholesterol sensors and modify expression of genes in pathways that govern transport, catabolism, and elimination of cholesterol.

Cholesterol is a major constituent of myelin and is thus essential for structure and function of the CNS. In addition, cholesterol plays a key role in CNS synaptogenesis and is essential for optimal neurotransmitter release (17). Defective cholesterol homeostasis in the brain is associated with neurological disease, especially neurodegenerative diseases (18). Most of the cholesterol in the CNS comes from *in situ* synthesis, and to maintain homeostasis, an equivalent amount of cholesterol must leave the brain. This output is to a large extent accounted for by the formation and excretion of 24(S)-hydroxycholesterol, which is secreted across the blood–brain barrier at high levels, particularly during the first two decades of human life (19). The role of 24(S)-hydroxycholesterol in the brain is particularly intriguing because patients with Alzheimer's disease have high circulating levels of 24(S)-hydroxycholesterol. This might simply be a reflection of the ongoing neurodegeneration, but it is also possible that dysregulation of cholesterol homeostasis in the brain contributes to the progression of the disease.

Although both LXR subtypes are expressed in the brain, LXRβ, in particular, is broadly expressed in the developing and adult rodent brain (20). Little is known about the functions of the LXRs in brain. In rat pheochromocytoma cells, the LXR agonists 22(R)-hydroxycholesterol and 5-tetradecyloxy-2-furancarboxylic acid induce neuronal differentiation as measured by neurite outgrowth (21). In primary astrocyte cultures, but not in primary neuronal cultures, LXR agonists enhance cholesterol efflux and regulate several established LXR target genes. Induction of these target genes was also confirmed by treating animals with LXR agonists (22).

LXRα and -β knockout mice have been generated, and the phenotypes of these mice suggest that LXRα and -β each has a distinct set of target genes and, therefore, they may have some nonoverlapping roles (1, 3, 10). To further identify the function of LXRs in the brain, in this study, we used double knockouts of LXRα and -β in mice and provided the first *in vivo* evidence that LXRs play important roles in cholesterol homeostasis in the brain. Furthermore, we show that loss of these two receptors leads to degenerative processes in the brain.

Materials and Methods

Animals. $LXR\alpha^{-/-}\beta^{-/-}$ mice were generated by gene targeting in our laboratory as described previously (23). All mice used in our study, $LXR\alpha^{-/-}\beta^{-/-}$ mice and wild-type ($LXR\alpha^{+/+}\beta^{+/+}$) controls, had mixed genetic backgrounds based on 129/Sv and C57BL/6 strains, finally backcrossed in C57BL/6 mice for three generations, unless otherwise stated. Animals were housed with a regular 12-h light/12-h dark cycle and fed a low-fat standard rodent chow diet (R36 Lactamin, Vadstena, Sweden) ad libitum, unless otherwise stated. Experiments were approved by the local ethical committee for animal experiments and the Guidelines for the Care and Use of Laboratory Animals were followed.

Gross Neuropathology and CNS Tissue Processing. Mice aged between 2 months and 2 years were studied. Mice were perfused transcardially with either 4% paraformaldehyde or the fixative containing 2% paraformaldehyde and 2.5% glutaraldehyde (in

Abbreviations: LXR, liver X receptor; CSF, cerebrospinal fluid; ABC, ATP-binding cassette transporter proteins; SREBP-1, sterol regulatory element-binding protein-1; MAP2, microtubule-associated protein; GFAP, glial fibrillary acidic protein; RTQ-PCR, quantitative real-time RT-PCR; Apo, apolipoprotein; LDLR, low-density lipoprotein receptor.

‖To whom correspondence should be addressed. E-mail: jan-ake.gustafsson@mednut.ki.se.

www.pnas.org/cgi/doi/10.1073/pnas.172510899

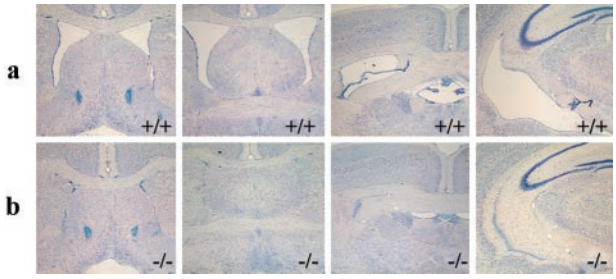

Fig. 1. Nissl-stained coronal sections show histology of old wild-type ($LXR\alpha^{+/+}\beta^{+/+}$) (*a*) and old $LXR\alpha^{-/-}\beta^{-/-}$ mice (*b*). Note the closed lateral ventricles in old $LXR\alpha^{-/-}\beta^{-/-}$ mice (original magnification: ×2.5).

0.1 M PBS, pH 7.4). Glutaraldehyde-fixed brains were postfixed in 2% osmium tetroxide, dehydrated, and embedded in LX-112. Brains perfused with 4% paraformaldehyde were postfixed in the same fixative overnight at 4°C and then either dehydrated in 20% sucrose or processed for paraffin embedding. To evaluate the ventricular system, coronal sections were cut.

Histopathology. Nissl and hematoxylin/eosin staining were used to examine the cytoarchitecture of brains with light microscopy. For myelin staining, the black–gold method was used as described (24). Lipid deposits were revealed by staining with oil red O on cryosections as previously described (25). To compare the ultrastructure of microvessels, microglia, neurons, and astrocytes of wild-type and $LXR\alpha^{-/-}\beta^{-/-}$ mice, several regions, including cerebral cortex, hippocampus, caudate putamen, globus pallidus, substantia nigra, cerebellum, lateral ventricle, third ventricle, and spinal cord, were cut as 0.8-μm semithin sections and stained with toluidine blue.

Immunohistochemistry. For immunohistochemistry, brain sections were stained as described (26). Paraffin sections (6 μm) were used for antimicrotubule-associated protein (MAP2) monoclonal mouse IgG1 antibody (1:500, Becton Dickinson); cryosections (30 μm) were used with the following antibodies: antiglial fibrillary acidic protein (GFAP) (1:500, Santa Cruz), anti-ApoE polyclonal antibody (1:1,000, Becton Dickinson), and anti-α smooth muscle actin (1:500, Sigma).

Ultrastructural Studies. Thin sections of LX-112-embedded tissue were cut with a diamond knife on a Reichert Ultracut ultramicrotome and mounted on hole-mesh copper grids, stained with uranyl acetate followed by lead citrate, and then viewed in a Leo 906 (Helsingborg, Sweden) electron microscope.

Morphometry. Morphometry was performed by using IMAGE-PRO PLUS software (Media Cybernetics, Silver Spring, MD). Ventricular size was compared in $LXR\alpha^{-/-}\beta^{-/-}$ mice and wild-type littermates at 14–18 months of age. One representative of all old $LXR\alpha^{-/-}\beta^{-/-}$ brains with decreased lateral ventricle is shown in Fig. 1, together with one control age-matched brain with regular lateral ventricles. Area of lateral ventricle was measured on six serial micrographs of the Nissl-stained coronal brain sections at the same magnification. Hematoxylin/eosin staining was used to determine the extent of vascularization on six level-matched micrographs in old mice. Vessels with an area greater than 40 (relative value) were counted, and percentage of vessels per micrograph was calculated. GFAP-stained sections were used to illustrate the number of astrocytes in substantia nigra and lateral globus pallidus. A mean value of the above was calculated for each animal, and statistical analysis was performed.

Quantitative Real-Time RT-PCR (RTQ-PCR). For RTQ-PCR, brains were obtained from 3-mo-old male mice fed a low-fat standard rodent chow diet, as well as from 10- to 12-mo-old male mice fed a control low-fat standard rodent chow diet or supplemented with 0.025% (wt/wt) of the synthetic LXR agonist T0901317 (7). Total RNA and cDNA were prepared as described (7). The real-time PCR reaction contained, in a final volume of 25 μl, 50 ng of cDNA and 12.5 μl of 2× SYBR Green PCR Master Mix (no. 4312704, PE Biosystems, Foster City, CA). RTQ-PCR was performed in triplicate by using ABI PRISM 7700 Sequence Detection System instrument and software (PE Applied Biosystems). RNA samples were normalized for comparison by determining 18S rRNA levels by Taqman real-time RT-PCR (PE Applied Biosystems). Data represent results from three to five individual animals. Primers were obtained from previous publications (27, 28). Sequences for additional primers, designed by using PRIMER EXPRESS software (PE Applied Biosystems), were as follows (5′-3′): ABCA2, GGT CCT GTC ACC CTC TCA GTA CC and AGC CGG AAT GTG CTC ACC; ABCG1, CTG GTG AGA GCC GTG CGA GAG G and CAG GCC GAT CCC AAT GTG CGA GGT G; ApoER2, AGT GTC CCG ATG GCT CTG AC and CAG CTT AAC TTC TCG GCA GGA; very low-density lipoprotein receptor (VLDLR), TGC GAG AGC CTG CCT CC and TCG CCC CAG TCT GAC CA.

Statistics. Data are presented as mean ± SEM.

Morphometry. The significance of differences between groups was tested by Student's *t* test.

RTQ-PCR. In Table 1, Experiment A, the significance of relative gene expression is indicated by *, $P < 0.05$ vs. wild-type control (Student's *t* test). In Table 1, Experiment B, the significance of relative gene expression is indicated by †, $P < 0.03$, according to Bonferroni correction, vs. wild-type control (two-way ANOVA, followed by post hoc comparisons according to Dunnett's tests or by nonorthogonal planned comparisons, respectively) (STATISTICA software, Stat Soft, Tulsa, OK). The values of the corresponding wild-type control group were arbitrarily assigned a value of 100.

Results

Closed Ventricular System. Both young wild-type and $LXR\alpha^{-/-}\beta^{-/-}$ mice have ventricles of normal size (data not shown). In 1-yr-old wild-type mice, serial coronal sections of brains show normal lateral ventricles with a continuous free space extending from the rostral to the caudal level (Fig. 1*a*). Similar sections from age-matched $LXR\alpha^{-/-}\beta^{-/-}$ mice are depicted in Fig. 1*b*. In these brains, the size of lateral ventricles is greatly decreased, with little empty space left. The third ventricle is closed (Fig. 2*b*), and just a very thin split can be seen in some animals. The dorsal third ventricle (Fig. 1*b*), cerebral aqueduct (Fig. 2*c*), fourth ventricle (Fig. 2*d*), and central canal of the spinal cord are also decreased in size, but the change is not as severe as that seen in the lateral and third ventricles. Morphometrical analysis indicated a significant decrease in the area of the lateral ventricles in $LXR\alpha^{-/-}\beta^{-/-}$ mice (143.5 ± 21.8) compared with wild-type (5,051.6 ± 55.1) ($P < 0.001$).

Abnormal Choroid Plexus Epithelial Cells and Ependymal Cells. The morphology of choroid plexus was examined on toluidine blue-stained semithin sections. In wild-type mice (Fig. 3*a*), the choroid plexus is clearly identified with numerous villi, lined with epithelial cells and with a connective tissue core in which blood vessels are present. No choroid plexus and no villi are detectable in $LXR\alpha^{-/-}\beta^{-/-}$ mice. Instead, there is a pale layer in the lateral ventricle, with an increased number of blood vessels (Fig. 3*b*).

Ultrastructural examination of wild-type mice shows a normal choroid plexus (Fig. 3*c*), where the epithelial cells are separated by an intercellular space with junctions at the apical end and at

Table 1. Relative amounts of mRNA of genes regulating cholesterol and lipid homeostasis in brains from wild-type ($LXR\alpha^{+/+}\beta^{+/+}$) and $LXR\alpha^{-/-}\beta^{-/-}$ mice

	Experiment A		Experiment B			
	WT (3 m)	$LXR\alpha^{-/-}\beta^{-/-}$ (3 m)	WT (10 m)	WT (10 m)	$LXR\alpha^{-/-}\beta^{-/-}$ (10 m)	$LXR\alpha^{-/-}\beta^{-/-}$ (10 m)
Tularik (T0901317)	−	−	−	+	−	+
ABCA1	100 ± 39	51 ± 15	100 ± 17	334 ± 52†	50 ± 6†	51 ± 15
ABCA2	100 ± 67	53 ± 11	100 ± 35	117 ± 24	97 ± 12	125 ± 14
ABCG1	100 ± 24	78 ± 32	100 ± 35	128 ± 3	41 ± 7†	39 ± 13
ABCG5	100 ± 67	72 ± 16	100 ± 35	133 ± 13	82 ± 51	75 ± 15
ABCG8	100 ± 17	66 ± 11*	100 ± 17	118 ± 24	55 ± 18†	55 ± 8
LDLR	100 ± 36	69 ± 3	100 ± 34	76 ± 23	55 ± 5†	38 ± 7
SREBP-2	100 ± 57	71 ± 20	100 ± 28	82 ± 19	52 ± 24†	66 ± 15
HMG-CoA synthase	100 ± 34	90 ± 6	100 ± 31	97 ± 13	88 ± 6	88 ± 18
HMG-CoA reductase	100 ± 50	62 ± 8	100 ± 23	80 ± 13	60 ± 14†	47 ± 14
FPP synthase	100 ± 35	65 ± 30	100 ± 9	96 ± 8	75 ± 9†	82 ± 4
Squalene synthase	100 ± 45	76 ± 3	100 ± 18	100 ± 19	70 ± 14†	63 ± 11
SREBP-1a	100 ± 35	81 ± 25	100 ± 23	110 ± 8	80 ± 6	93 ± 13
SREBP-1c	100 ± 57	69 ± 51	100 ± 29	135 ± 39	21 ± 5†	16 ± 4
Acetyl-CoA carboxylase	100 ± 46	92 ± 13	100 ± 32	67 ± 25	67 ± 36	18 ± 11
Fatty acid synthase	100 ± 44	58 ± 11	100 ± 43	150 ± 13†	81 ± 13	135 ± 20
SCD-1	100 ± 38	51 ± 20	100 ± 60	130 ± 29	19 ± 3†	61 ± 24
ApoE	100 ± 23	91 ± 14	100 ± 31	131 ± 11	99 ± 8	128 ± 18
ApoER2	100 ± 27	85 ± 19	100 ± 18	115 ± 19	105 ± 12	132 ± 18
VLDLR	100 ± 25	83 ± 13	100 ± 25	96 ± 17	77 ± 13	80 ± 24

m, month of age; HMG, hydroxymethylglutaryl; FPP, fernesyl pyrophosphate.
*$P < 0.05$ vs wild-type control.
†$P < 0.03$ vs. wild-type control.

the base. Numerous microvilli are projecting from the apical part of the cells, and the cytoplasm contains normal mitochondria. Very little lipofuscin can be seen. The extracellular matrix containing collagen separates the epithelial cells from the adjacent arteriolar segment. Ependymal cells with microvilli are separated from the choroid epithelial cells by a space filled with cerebrospinal fluid (CSF). In $LXR\alpha^{-/-}\beta^{-/-}$ mice, no visible space exists between ependymal cells and choroid epithelial cells. The cytoplasm of choroid epithelial cells is full of lipid vacuoles, and mitochondria are smaller compared with wild type (Fig. 3*d*). Ependymal cells, especially those around the third ventricle and cerebral aqueduct, are swollen and also contain large lipid vacuoles (data not shown).

Lipid Accumulation Around the Blood–CSF Barrier, the Blood–Brain Barrier, and Specific Brain Areas. Oil red O staining shows moderately stained bundles of nerve fibers in both wild-type and $LXR\alpha^{-/-}\beta^{-/-}$ young mice. In old $LXR\alpha^{-/-}\beta^{-/-}$ mice, intensely stained lipid components appear in regions around the blood–CSF barrier, i.e., the lateral ventricle (Fig. 2*a*), third ventricle (Fig. 2*b*), cerebral aqueduct (Fig. 2*c*), fourth ventricle (Fig. 2*d*), median eminence (Fig. 2*e*), subfornical organ, and organum vasculosum of the lamina terminalis, as well as the pars reticularis of substantia nigra (Fig. 4*b*), globus pallidus, and subthalamic nucleus. In these regions, there are no lipid droplets in age-matched wild-type mice (Fig. 4*a*). Lipid-laden cells are located mainly around the blood vessels (Fig. 2*f*).

Toluidine blue staining shows cholesterol clefts (Fig. 4*f*) and foamy cells (Fig. 4*g*) in the pars reticularis of substantia nigra. Ultrastructral examination reveals this region to be severely destroyed by lipid crystal clefts (Fig. 5*e*). Foamy cells are full of lipid remnants, with few organelles left (Fig. 5*f*). A few small lipid droplets also appear in the cerebral cortex, hippocampus, cerebellum, and spinal cord, but the staining here is not as

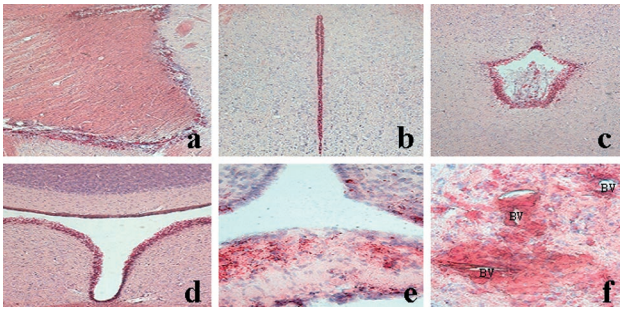

Fig. 2. Oil red O staining shows accumulation of lipid droplets in old $LXR\alpha^{-/-}\beta^{-/-}$ mice. Lipid-laden cells are located mainly around: (*a*) lateral ventricle; (*b*) third ventricle; (*c*) cerebral aqueduct; (*d*) fourth ventricle; (*e*) median eminence; and (*f*) microvessels (BV) in substantia nigra pars reticularis. (Original magnifications: ×10 in *a*–*e*; ×40 in *f*.)

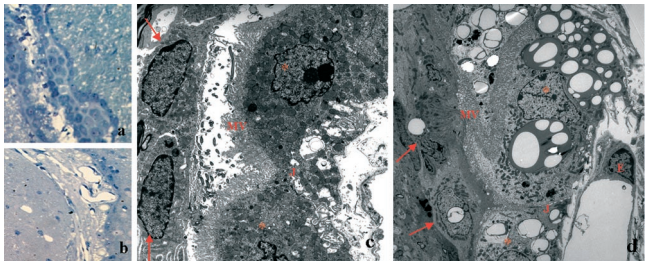

Fig. 3. Toluidine blue staining shows no clear choroid plexus in $LXR\alpha^{-/-}\beta^{-/-}$ mice (*b*) compared with wild-type mice (*a*). The electron micrograph shows normal choroid plexus epithelial cells (asterisks) and ependymal cells (arrows) from wild-type mice (*a*). In $LXR\alpha^{-/-}\beta^{-/-}$ mice, choroid plexus epithelial cells (asterisks) and ependymal cells (arrows) around lateral ventricle are full of lipid vacuoles (*d*). MV, microvilli; J, junction; E, endothelium. (Original magnifications: ×10 in *a* and *b*; ×3,597in *c* and *d*.)

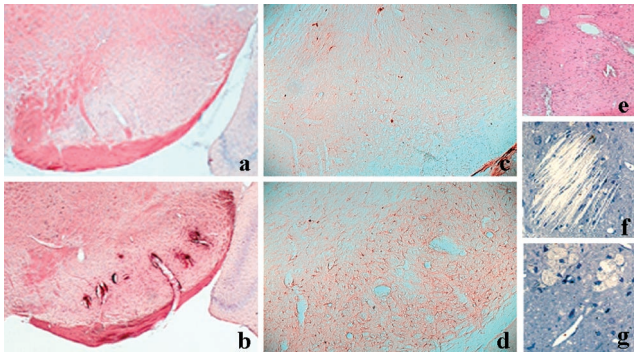

Fig. 4. In substantia nigra pars reticularis, oil red O staining shows lipid accumulation around the abnormal vessels in $LXR\alpha^{-/-}\beta^{-/-}$ mice (*b*), no lipid staining in wild-type mice (*a*). GFAP immunostaining shows the increase in number of GFAP immunoreactive cells in $LXR\alpha^{-/-}\beta^{-/-}$ mice (*d*) compared with wild-type mice (*c*). Hematoxylin/eosin staining shows the enlarged and distorted vessels in $LXR\alpha^{-/-}\beta^{-/-}$ mice (*e*). Toluidine blue staining shows cholesterol clefts (*f*) and foamy cells (*g*) in $LXR\alpha^{-/-}\beta^{-/-}$ mice. (Original magnifications: ×2.5 in *a* and *b*; ×10 in *c*–*e*; ×40 in *f* and *g*.)

intense. Because the abnormality is observed only in old animals, these have been examined in detail and are described below.

Blood Vessel Pathology. By Nissl staining, no microvessels can be seen in wild-type mice, whereas malformed blood vessels with enlarged size and distorted shape can be identified in $LXR\alpha^{-/-}\beta^{-/-}$ littermates (data not shown). Hematoxylin/eosin staining confirmed an increase in both number and size of blood vessels in $LXR\alpha^{-/-}\beta^{-/-}$ mice (Fig. 4*e*). In some $LXR\alpha^{-/-}\beta^{-/-}$ animals, evidence of previous hemorrhage can be seen in the thalamus, globus pallidus, pontin, and hippocampus (data not shown). Morphometric analysis confirmed that there is a significant increase in the area of blood vessels in $LXR\alpha^{-/-}\beta^{-/-}$ mice (3.78 ± 0.56) compared with wild type (0.22 ± 0.02) ($P < 0.001$).

The ultrastructure of microvessels in several brain regions was analyzed. More than half of the microvessels in the substantia nigra and globus pallidus show severe abnormality. Fewer microvessels in hippocampus and cerebellum are affected, whereas few microvessels are affected in the cerebral cortex. As shown in Fig. 5*a*, microvessels in wild-type mice contain endothelial cells and pericytes, and astrocytic feet are attached to the abluminal surface of the vessels. A normal tight junction seals the space between the endothelial surfaces. In $LXR\alpha^{-/-}\beta^{-/-}$ mice, endothelial cells and tight junctions appear to be normal, but pericytes contain lipofuscin. The extracellular matrix contains many thick and disorganized collagen bundles in the vicinity of the vessels, indicating abundant microvascular fibrosis. Irregular fibrillar structures extend from the outer aspect of the collagen bundles. Astrocytic feet are swollen and contain many pale lipid vacuoles and myelin-like inclusions (Figs. 5*b*). In the smooth muscle cells, some actin structure remains, but cells are loaded with pale lipid vacuoles (data not shown). Immunostaining for α smooth muscle actin shows much less staining in $LXR\alpha^{-/-}\beta^{-/-}$ mice. In the smaller brain vessels, there is clear α smooth muscle actin immunoreactivity in wild-type mice, whereas in $LXR\alpha^{-/-}\beta^{-/-}$ mice, no staining is evident. In larger blood vessels, for example those in the cortex, weaker staining is seen in $LXR\alpha^{-/-}\beta^{-/-}$ mice (data not shown).

Neurodegeneration and Axonal Dysmyelination. From the Nissl-stained sections, it is clear that there are less neurons in the substantia nigra and globus pallidus of $LXR\alpha^{-/-}\beta^{-/-}$ than in wild-type littermates (data not shown). GFAP immunostaining shows that reduction in neurons is accompanied by an increase in the number of astrocytes in these regions (Fig. 4*d*) compared

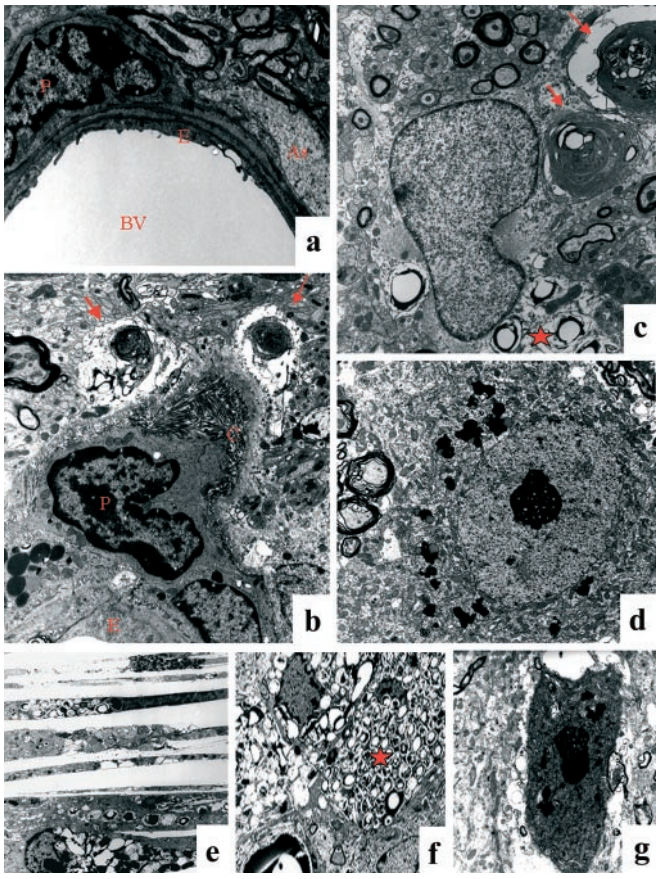

Fig. 5. The electron micrograph shows a normal blood vessel (BV) in wild-type mice (*a*). Endothelium (E) is surrounded by pericyte (P) and astrocytic feet (As). Vessel from $LXR\alpha^{-/-}\beta^{-/-}$ mice (*b*) shows disorganized collagen bundles (C) surrounding the pericyte and swollen astrocytic feet with myelin-like inclusions (arrows). Astrocyte contains lipid vacuoles (star) (*c*). Macrophage/microglia is full of lipid vacuoles (star) (*f*). Cholesterol clefts are seen in substantia nigra pars reticularis (*e*). Normal neuronal morphology in wild-type mice (*d*), degenerated neurons in $LXR\alpha^{-/-}\beta^{-/-}$ mice (*g*). (Original magnifications: ×4,646 in *a* and *b*; ×6,000 in *c*; ×3,597 in *d*; ×3,597 in *e*; ×2,784 in *f*; ×6,000 in *g*.)

with wild type (Fig. 4*c*). The increase in astrocytes is statistically significant in $LXR\alpha^{-/-}\beta^{-/-}$ ($1{,}595.6 \pm 287.6$) compared with wild type (64.6 ± 23.9) ($P < 0.001$). Specific neuronal markers, like MAP2, were also used to document the neuronal deficit. As shown in Fig. 6*a*, MAP2-stained cytoplasm and dendrites of neurons in substantia nigra pars reticularis of wild-type mice, and there is obvious reduction of both MAP2 immunoreactive cell bodies and neurites in $LXR\alpha^{-/-}\beta^{-/-}$ mice (Fig. 6*b*).

By electron microscopy, neurons in wild-type mice appear to have normal morphology (Fig. 5*d*), whereas in $LXR\alpha^{-/-}\beta^{-/-}$ mice, there were many dark-colored neurons around the impaired blood vessels (Fig. 5*g*). These neurons exhibit morphology displaying nuclear and cytoplasmic condensation with condensed and packed ribosomes and lipofuscin in the cytoplasm. Mitochondria appear to be intact, but the Golgi apparatus is swollen or condensed, and plasma and nuclear membrane are ruffled. Astrocytes contain many lipid vacuoles and myelin-like or laminar-like structures (Fig. 5*c*).

With the black–gold histological method shown in Fig. 6*c* from wild-type and Fig. 6*d* from $LXR\alpha^{-/-}\beta^{-/-}$ mice, there is a moderate reduction in the size of myelinated axons in $LXR\alpha^{-/-}\beta^{-/-}$ mice, but electron microscopic analysis did not demonstrate any demyelination in $LXR\alpha^{-/-}\beta^{-/-}$ mice. How-

NEUROSCIENCE

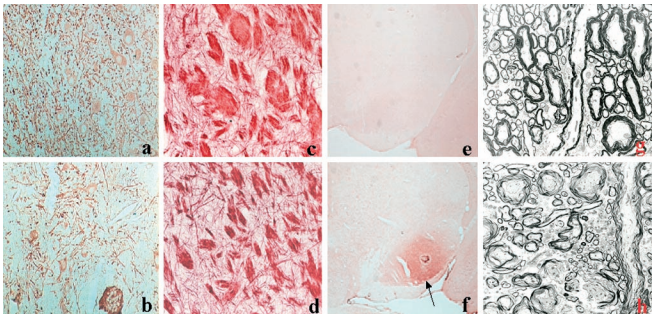

Fig. 6. MAP2 immunostaining shows less positive neurons and their dendrites in $LXR\alpha^{-/-}\beta^{-/-}$ mice (*b*) compared with wild-type mice (*a*) in substantia nigra pars reticularis. Black–gold-stained myelin in this region in wild-type (*c*) and $LXR\alpha^{-/-}\beta^{-/-}$ mice (*d*). In e, no ApoE immunostaining is seen in substantia nigra pars reticularis in wild-type mice, whereas the arrow indicates strong ApoE immunostaining in this region in $LXR\alpha^{-/-}\beta^{-/-}$ mice (*f*). The electron micrograph shows the dysmyelination in $LXR\alpha^{-/-}\beta^{-/-}$ (*h*) compared with wild-type mice (*g*). (Original magnifications: ×40 in *a–d*; ×2.5 in *e* and *f*; ×2,784 in *g* and *h*.)

ever, in axons with larger diameter (Fig. 6*h*), lipid vacuoles are often seen among the bundles of myelinated axons, and global dysmyelination with thin uncompacted myelin sheaths without major dense lines is seen compared with wild-type littermates (Fig. 6*g*).

ApoE is produced by astrocytes in the CNS and is involved in transport of cholesterol. Interestingly, in $LXR\alpha^{-/-}\beta^{-/-}$ mice, ApoE is strongly expressed in lipid-laden regions like substantia nigra (Fig. 6*f*) and cells around the lateral ventricle. In addition, there is accumulation of ApoE around some blood vessels in the cerebral cortex in $LXR\alpha^{-/-}\beta^{-/-}$ mice. The diffuse ApoE staining indicates that this protein is not restricted within the cytoplasm. In wild-type mice, few ApoE-positive cells are found around blood vessels in cerebral cortex, and there is no staining in substantia nigra (Fig. 6*e*).

LXR Regulated Genes. To investigate the role of both LXRs in regulating cholesterol and lipid homeostasis in the brain, we determined the relative RNA expression of genes involved in cholesterol biosynthesis, cholesterol efflux, lipoprotein metabolism, and fatty acid biosynthesis, by RTQ-PCR. In 3-mo-old $LXR\alpha^{-/-}\beta^{-/-}$ mice, expression of the cholesterol transporters ABCA1, -A2, -G1, and -G5 was reduced by 50–20% [P = not significant (NS)] and that of ABCG8, another cholesterol transporter, by 66 ± 11% ($P < 0.05$) (Table 1, Experiment A). Treatment with LXR agonist T09001317 resulted in a 3.34 ± 5.2 ($P < 0.03$)-fold induction of ABCA1 expression in the brain of wild-type mice (not shown). Compared with untreated wild-type controls, the RNA levels of ABCA1, -G1, and -G8 were significantly decreased to 50 ± 6, 41 ± 7, and 55 ± 18% ($P < 0.03$), respectively, in untreated $LXR\alpha^{-/-}\beta^{-/-}$ mice (Table 1, Experiment B). Surprisingly, in neither of the two experiments were any significant changes in ApoE, ApoE receptor 2, or VLDLR expression seen, whereas a reduced expression of LDLR was seen in both 3- and 10-mo-old LXR double mutant mice, by 69 ± 3% (P = NS) and 55 ± 5% ($P < 0.03$), respectively (Table 1, Experiments A and B). Significantly fewer transcripts of SREBP-2 (52 ± 24%, $P < 0.03$), hydroxymethylglutaryl-CoA reductase (60 ± 14%, $P < 0.03$), farnesyl pyrophosphate synthase (75 ± 9%, $P < 0.03$), and Squalene synthase (70 ± 14%, $P < 0.03$) were detected in the brain of 10-mo-old untreated $LXR\alpha^{-/-}\beta^{-/-}$ mice than in wild-type controls (Table 1, Experiment B). The mRNA levels of SREBP-1c (21 ± 5%, $P < 0.03$), stearoyl CoA desaturase-1 (19 ± 3%, $P < 0.03$), but not of acetyl CoA decarboxylase and fatty acid synthase, were reduced in untreated $LXR\alpha^{-/-}\beta^{-/-}$ mice (Table 1, Experiment B).

Discussion

In the present study, we show that absence of LXRs in mice leads to disturbances in lipid homeostasis in the CNS and age-related neuropathological changes. The characteristic features of the brains of $LXR\alpha^{-/-}\beta^{-/-}$ mice are accumulation of lipid droplets and closure of ventricles. Ultrastructurally, epithelial cells of the choroid plexus and ependymal cells are filled with lipid droplets. The choroid plexus, situated inside the cerebral ventricles, is the site of the blood–CSF barrier (29). The choroid plexus is responsible for synthesis and secretion of CSF and for active and selective transport of substances to and from the CSF (30). The morphological changes of the choroid plexus in $LXR\alpha^{-/-}\beta^{-/-}$ mice suggest that alteration of secretion and filtration of this organ might be responsible for the closure of the ventricular system.

No expression of LXRs has been reported (20, 31) in the choroid plexus or ependymal cells, but in this study we have demonstrated the importance of LXRs in the function of the choroid plexus. Whether this is an indirect effect due to overall dysregulation of genes involved in cholesterol homeostasis remains to be determined. Modification of the choroid plexus with age is related to a lower rate of CSF secretion in elderly individuals (32, 33). In Alzheimer's disease, there is thickening of the basement membrane of the choroid plexus and flattening of epithelial cells. These changes are correlated with pathogenesis of late-onset Alzheimer's disease (34). Our data suggest that loss of LXR exacerbates age-related changes in the choroid plexus.

As $LXR\alpha^{-/-}\beta^{-/-}$ mice age, there are more brain blood vessels and more dilated vessels in the pars reticularis of the substatia nigra. Similar findings have been reported in brains of mice after chronic hypoxia (35). Because the ventricles are closed, many changes observed in the brain of $LXR\alpha^{-/-}\beta^{-/-}$ mice could be due to hypoxia.

The abnormalities in the blood vessels themselves could also lead to hypoxia. The smooth muscle cells around blood microvessels expressed very little smooth muscle actin and contained lipid vacuoles. Surrounding the vessels, there were distorted collagen deposits. The affected blood vessels might lose their contractile ability and would be susceptible to ruptures, which could explain the frequently observed hemorrhages in the brains of $LXR\alpha^{-/-}\beta^{-/-}$ mice. The response of the brain to such conditions would be increased angiogenesis, which might explain why there are more vessels in the brains of $LXR\alpha^{-/-}\beta^{-/-}$ mice. The cerebral microvascular system is known to be subject to senescence (36). Additional risk factors like Alzheimer's disease can accelerate the degeneration of capillaries (37). It seems that LXRs are also involved in this process.

In $LXR\alpha^{-/-}\beta^{-/-}$ mice, the most severe neuropathological changes occurred in specific brain areas, including the pars reticularis of substantia nigra, globus pallidus, and subthalamic nucleus. In these areas, blood vessels were enlarged and surrounded by lipid deposits. There was neuronal loss and astrocyte proliferation. Ultrastructural analyses showed that lipid inclusions were mainly localized in perivascular astrocytes and only few microglia/macrophages. Multiple dispersed intracellular lipid crystal structures severely destroyed the cytoplasmic architecture. Many neurons surrounding the abnormal microvessels showed evidence of degeneration. In the cerebral cortex, hippocampus, and cerebellum, there were a few lipid droplets deposited around blood vessels but no obvious degenerative changes.

There are a number of instances in which disturbance of cholesterol metabolism in the CNS may be etiologically related to the onset of neurological diseases (38–40). In ApoE knockout mice of advancing age, there is also lipid deposition in astrocytes in the globus pallidus and substantia nigra (41). Expression of

ApoE has been shown to be regulated by LXRs in macrophages and adipocytes (42). In the CNS, ApoE is secreted by astrocytes and is the carrier that transports and redistributes cholesterol via brain interstitial fluid to cells that express ApoB or -E (low-density lipoprotein) receptors (43). By immunohistochemistry, instead of a loss, we found a substantial accumulation of ApoE protein in substantia nigra of LXR$\alpha^{-/-}\beta^{-/-}$ mice. It therefore appears that loss of ApoE cannot explain the phenotype of LXR-deficient mice.

By RTQ-PCR, using mRNA extracted from whole brains, no change in levels of mRNA of ApoE was detected, indicating that the increased expression observed in immunohistochemical studies is posttranscriptional. Although ApoE is a key factor in the transport of cholesterol in some specific brain regions like substantia nigra, there are other proteins whose functions are essential for cholesterol homeostasis in the brain. Indeed, we found that expression of several established LXR target genes was significantly decreased in brains of *LXR*$\alpha^{-/-}\beta^{-/-}$ mice. These include ABCA1, -G1, and -G8, SREBP-1c and -2, LDLR, hydroxymethylglutaryl-CoA reductase, farnesyl pyrophosphate synthase, Squalene synthase, and stearoyl CoA desaturase-1. In glial cultures, LXR agonists have been shown to induce expression of some of these target genes and to stimulate cholesterol efflux (22). Hence the ABC transporters may be involved in actively extruding cholesterol from astroglial cells in CNS, especially perivascular astrocytes.

One observation that needs to be emphasized is that not all astrocytes but only perivascular astrocytes are lipid laden. Brain capillary endothelial cells express LDLR and expression is modulated by astrocytes (44). It is possible that defective transport of cholesterol could be due to low levels of LDLR in endothelial cells, as well as neurons.

In conclusion, our data suggest that mutation of LXRs affects the brain–CSF barrier and the blood–brain barrier and leads to neurodegeneration in specific brain regions. The defect may be due to alteration of lipid homeostasis in CNS; however, it is also possible that changes in net lipid homeostasis in the whole animal may, indirectly, contribute to the defect of CNS. It has been shown that treating humans with agents that block cholesterol synthesis in every organ, including the brain, markedly reduces the incidence of Alzheimer's disease (45). It is also noteworthy that the neuropathological changes were evident only in older mice. These mice could, therefore, be valuable for studying the mechanisms underlying age-related neurodegeneration under conditions of abnormal lipid homeostasis. Such investigations may provide insight into whether pharmacological intervention, with LXRs as targets, could constitute novel treatments for lipid disorders and neurodegenerative diseases.

This project was funded by the Swedish Science Council and by grants from Tore Nilson and Thuring Foundations (Stockholm) and KaroBio AB.

1. Peet, D. J., Janowski, B. A. & Mangelsdorf, D. J. (1998) *Curr. Opin. Genet. Dev.* **8,** 571–575.
2. Janowski, B. A., Willy, P. J., Devi, T. R., Falck, J. R. & Mangelsdorf, D. J. (1996) *Nature* **383,** 728–731.
3. Lehmann, J. M., Kliewer, S. A., Moore, L. B., Smith-Oliver, T. A., Oliver, B. B., Su, J. L., Sundseth, S. S., Winegar, D. A., Blanchard, D. E., Spencer, T. A., *et al.* (1997) *J. Biol. Chem.* **272,** 3137–3140.
4. Fu, X., Menke, J. G., Chen, Y., Zhou, G., MacNaul, K. L., Wright, S. D., Sparrow, C. P. & Lund, E. G. (2001) *J. Biol. Chem.* **276,** 38378–38387.
5. Yeagle, P. L. (1985) *Biochim. Biophys. Acta* **822,** 267–287.
6. Lu, T. T., Repa, J. J. & Mangelsdorf, D. J. (2001) *J. Biol. Chem.* **276,** 37735–37738.
7. Repa, J. J., Liang, G., Ou, J., Bashmakov, Y., Lobaccaro, J. M., Shimomura, I., Shan, B., Brown, M. S., Goldstein, J. L. & Mangelsdorf, D. J. (2000) *Genes Dev.* **14,** 2819–2830.
8. Schultz, J. R., Tu, H., Luk, A., Repa, J. J., Medina, J. C., Li, L., Schwendner, S., Wang, S., Thoolen, M., Mangelsdorf, D. J., *et al*. (2000) *Genes Dev.* **14,** 2831–2838.
9. Peet, D. J., Turley, S. D., Ma, W., Janowski, B. A., Lobaccaro, J. M., Hammer, R. E. & Mangelsdorf, D. J. (1998) *Cell* **93,** 693–704.
10. Edwards, P. A., Kast, H. R. & Anisfeld, A. M. (2002) *J. Lipid Res.* **43,** 2–12.
11. Zhang, Y., Yin, L. & Hillgartner, F. B. (2001) *J. Biol. Chem.* **276,** 974–983.
12. Joseph, S. B., Laffitte, B. A., Patel, P. H., Watson, M. A., Matsukuma, K. E., Walczak, R., Collins, J. L., Osborne, T. F. & Tontonoz, P. (2002) *J. Biol. Chem.* **277,** 11019–11025.
13. Repa, J. J., Turley, S. D., Lobaccaro, J. A., Medina, J., Li, L., Lustig, K., Shan, B., Heyman, R. A., Dietschy, J. M. & Mangelsdorf, D. J. (2000) *Science* **289,** 1524–1529.
14. Costet, P., Luo, Y., Wang, N. & Tall, A. R. (2000) *J. Biol. Chem.* **275,** 28240–28245.
15. Venkateswaran, A., Repa, J. J., Lobaccaro, J. M., Bronson, A., Mangelsdorf, D. J. & Edwards, P. A. (2000) *J. Biol. Chem.* **275,** 14700–14707.
16. Laffitte, B. A., Joseph, S. B., Walczak, R., Pei, L., Wilpitz, D. C., Collins, J. L. & Tontonoz, P. (2001) *Mol. Cell. Biol.* **21,** 7558–7568.
17. Mauch, D. H., Nagler, K., Schumacher, S., Goritz, C., Muller, E. C., Otto, A. & Pfrieger, F. W. (2001) *Science* **294,** 1354–1357.
18. Dietschy, J. M. & Turley, S. D. (2001) *Curr. Opin. Lipidol.* **12,** 105–112.
19. Lutjohann, D., Breuer, O., Ahlborg, G., Nennesmo, I., Siden, A., Diczfalusy, U. & Bjorkhem, I. (1996) *Proc. Natl. Acad. Sci. USA* **93,** 9799–9804.
20. Kainu, T., Kononen, J., Enmark, E., Gustafsson, J. A. & Pelto-Huikko, M. (1996) *J. Mol. Neurosci.* **7,** 29–39.
21. Schmidt, A., Vogel, R., Holloway, M. K., Rutledge, S. J., Friedman, O., Yang, Z., Rodan, G. A. & Friedman, E. (1999) *Mol. Cell. Endocrinol.* **155,** 51–60.
22. Whitney, K. D., Watson, M. A., Collins, J. L., Benson, W. G., Stone, T. M., Numerick, M. J., Tippin, T. K., Wilson, J. G., Winegar, D. A. & Kliewer, S. A. (2002) *Mol. Endocrinol.* **16,** 1378–1385.
23. Alberti, S., Schuster, G., Parini, P., Feltkamp, D., Diczfalusy, U., Rudling, M., Angelin, B., Bjorkhem, I., Pettersson, S. & Gustafsson, J. A. (2001) *J. Clin. Invest.* **107,** 565–573.
24. Schmued, L. & Slikker, W., Jr. (1999) *Brain Res.* **837,** 289–297.
25. Nicoletti, A., Kaveri, S., Caligiuri, G., Bariety, J. & Hansson, G. K. (1998) *J. Clin. Invest.* **102,** 910–918.
26. Wang, L., Andersson, S., Warner, M. & Gustafsson, J. A. (2001) *Proc. Natl. Acad. Sci. USA* **98,** 2792–2796.
27. Yang, J., Goldstein, J. L., Hammer, R. E., Moon, Y. A., Brown, M. S. & Horton, J. D. (2001) *Proc. Natl. Acad. Sci. USA* **98,** 13607–13612.
28. Liang, C. P. & Tall, A. R. (2001) *J. Biol. Chem.* **276,** 49066–49076.
29. Oldendorf, W. H. & Davson, H. (1967) *Trans. Am. Neurol. Assoc.* **92,** 123–127.
30. Segal, M. B. (2000) *Cell. Mol. Neurobiol.* **20,** 183–196.
31. Teboul, M., Enmark, E., Li, Q., Wikstrom, A. C., Pelto-Huikko, M. & Gustafsson, J. A. (1995) *Proc. Natl. Acad. Sci. USA* **92,** 2096–2100.
32. May, C., Kaye, J. A., Atack, J. R., Schapiro, M. B., Friedland, R. P. & Rapoport, S. I. (1990) *Neurology* **40,** 500–503.
33. Preston, J. E. (2001) *Microsc. Res. Technol.* **52,** 31–37.
34. Serot, J. M., Bene, M. C., Foliguet, B. & Faure, G. C. (2000) *Acta Neuropathol. (Berlin)* **99,** 105–108.
35. Boero, J. A., Ascher, J., Arregui, A., Rovainen, C. & Woolsey, T. A. (1999) *J. Appl. Physiol.* **86,** 1211–1219.
36. Farkas, E. & Luiten, P. G. (2001) *Prog. Neurobiol.* **64,** 575–611.
37. Kalaria, R. N. (2002) *Cerebrovasc. Dis.* **13,** Suppl. 2, 48–52.
38. Irons, M., Elias, E. R., Tint, G. S., Salen, G., Frieden, R., Buie, T. M. & Ampola, M. (1994) *Am. J. Med. Genet.* **50,** 347–352.
39. Masliah, E., Mallory, M., Ge, N., Alford, M., Veinbergs, I. & Roses, A. D. (1995) *Exp. Neurol.* **136,** 107–122.
40. Xie, C., Burns, D. K., Turley, S. D. & Dietschy, J. M. (2000) *J. Neuropathol. Exp. Neurol.* **59,** 1106–1117.
41. Mato, M., Ookawara, S., Mashiko, T., Sakamoto, A., Mato, T. K., Maeda, N. & Kodama, T. (1999) *Anat. Rec.* **256,** 165–176.
42. Laffitte, B. A., Repa, J. J., Joseph, S. B., Wilpitz, D. C., Kast, H. R., Mangelsdorf, D. J. & Tontonoz, P. (2001) *Proc. Natl. Acad. Sci. USA* **98,** 507–512.
43. Pitas, R. E., Boyles, J. K., Lee, S. H., Foss, D. & Mahley, R. W. (1987) *Biochim. Biophys. Acta* **917,** 148–161.
44. Dehouck, B., Dehouck, M. P., Fruchart, J. C. & Cecchelli, R. (1994) *J. Cell Biol.* **126,** 465–473.
45. Wolozin, B., Kellman, W., Ruosseau, P., Celesia, G. G. & Siegel, G. (2000) *Arch. Neurol.* **57,** 1439–1443.